Three flavor neutrino oscillation analysis of atmospheric neutrinos in Super-Kamiokande

J. Hosaka,[1] K. Ishihara,[1] J. Kameda,[1] Y. Koshio,[1] A. Minamino,[1] C. Mitsuda,[1] M. Miura,[1] S. Moriyama,[1] M. Nakahata,[1] T. Namba,[1] Y. Obayashi,[1] M. Shiozawa,[1] Y. Suzuki,[1] A. Takeda,[1] Y. Takeuchi,[1] S. Yamada,[1] I. Higuchi,[2] M. Ishitsuka,[2] T. Kajita,[2] K. Kaneyuki,[2] G. Mitsuka,[2] S. Nakayama,[2] H. Nishino,[2] A. Okada,[2] K. Okumura,[2] C. Saji,[2] Y. Takenaga,[2] S. Clark,[3] S. Desai,[3,*] E. Kearns,[3] S. Likhoded,[3] J. L. Stone,[3] L. R. Sulak,[3] W. Wang,[3] M. Goldhaber,[4] D. Casper,[5] J. P. Cravens,[5] W. R. Kropp,[5] D. W. Liu,[5] S. Mine,[5] C. Regis,[5] M. B. Smy,[5] H. W. Sobel,[5] C. W. Sterner,[5] M. R. Vagins,[5] K. S. Ganezer,[6] J. E. Hill,[6] W. E. Keig,[6] J. S. Jang,[7] J. Y. Kim,[7] I. T. Lim,[7] K. Scholberg,[8] C. W. Walter,[8] R. Wendell,[8] R. W. Ellsworth,[9] S. Tasaka,[10] E. Guillian,[11] A. Kibayashi,[11] J. G. Learned,[11] S. Matsuno,[11] M. D. Messier,[12] Y. Hayato,[13,†] A. K. Ichikawa,[13] T. Ishida,[13] T. Ishii,[13] T. Iwashita,[13] T. Kobayashi,[13] T. Nakadaira,[13] K. Nakamura,[13] K. Nitta,[13] Y. Oyama,[13] Y. Totsuka,[13] A. T. Suzuki,[14] M. Hasegawa,[15] I. Kato,[15,‡] H. Maesaka,[15] T. Nakaya,[15] K. Nishikawa,[15] T. Sasaki,[15] H. Sato,[15] S. Yamamoto,[15] M. Yokoyama,[15] T. J. Haines,[16,5] S. Dazeley,[17] S. Hatakeyama,[17] R. Svoboda,[17] E. Blaufuss,[18] J. A. Goodman,[18] G. W. Sullivan,[18] D. Turcan,[18] J. Cooley,[19] A. Habig,[20] Y. Fukuda,[21] T. Sato,[21] Y. Itow,[22] C. K. Jung,[23] T. Kato,[23] K. Kobayashi,[23] M. Malek,[23] C. Mauger,[23] C. McGrew,[23] A. Sarrat,[1,23] C. Yanagisawa,[23] N. Tamura,[24] M. Sakuda,[25] Y. Kuno,[26] M. Yoshida,[26] S. B. Kim,[27] J. Yoo,[27] T. Ishizuka,[28] H. Okazawa,[29] Y. Choi,[30] H. K. Seo,[30] Y. Gando,[31] T. Hasegawa,[31] K. Inoue,[31] J. Shirai,[31] A. Suzuki,[31] K. Nishijima,[32] H. Ishino,[33] Y. Watanabe,[33] M. Koshiba,[34] D. Kielczewska,[35,5] J. Zalipska,[35] H. G. Berns,[36] R. Gran,[36,20] K. K. Shiraishi,[36] A. Stachyra,[36] K. Washburn,[36] and R. J. Wilkes[36]

(Super-Kamiokande Collaboration)

[1]*Kamioka Observatory, Institute for Cosmic Ray Research, University of Tokyo, Kamioka, Gifu, 506-1205, Japan*
[2]*Research Center for Cosmic Neutrinos, Institute for Cosmic Ray Research, University of Tokyo, Kashiwa, Chiba 277-8582, Japan*
[3]*Department of Physics, Boston University, Boston, Massachusetts 02215, USA*
[4]*Physics Department, Brookhaven National Laboratory, Upton, New York 11973, USA*
[5]*Department of Physics and Astronomy, University of California, Irvine, Irvine, California 92697-4575, USA*
[6]*Department of Physics, California State University, Dominguez Hills, Carson, California 90747, USA*
[7]*Department of Physics, Chonnam National University, Kwangju 500-757, Korea*
[8]*Department of Physics, Duke University, Durham, North Carolina 27708 USA*
[9]*Department of Physics, George Mason University, Fairfax, Virginia 22030, USA*
[10]*Department of Physics, Gifu University, Gifu, Gifu 501-1193, Japan*
[11]*Department of Physics and Astronomy, University of Hawaii, Honolulu, Hawaii 96822, USA*
[12]*Department of Physics, Indiana University, Bloomington, Indiana 47405-7105, USA*
[13]*High Energy Accelerator Research Organization (KEK), Tsukuba, Ibaraki 305-0801, Japan*
[14]*Department of Physics, Kobe University, Kobe, Hyogo 657-8501, Japan*
[15]*Department of Physics, Kyoto University, Kyoto 606-8502, Japan*
[16]*Physics Division, P-23, Los Alamos National Laboratory, Los Alamos, New Mexico 87544, USA*
[17]*Department of Physics and Astronomy, Louisiana State University, Baton Rouge, Louisiana 70803, USA*
[18]*Department of Physics, University of Maryland, College Park, Maryland 20742, USA*
[19]*Department of Physics, Massachusetts Institute of Technology, Cambridge, Massachusetts 02139, USA*
[20]*Department of Physics, University of Minnesota, Duluth, Minnesota 55812-2496, USA*
[21]*Department of Physics, Miyagi University of Education, Sendai,Miyagi 980-0845, Japan*
[22]*Solar-Terrestrial Environment Laboratory, Nagoya University, Nagoya, Aichi 464-8601, Japan*
[23]*Department of Physics and Astronomy, State University of New York, Stony Brook, New York 11794-3800, USA*
[24]*Department of Physics, Niigata University, Niigata, Niigata 950-2181, Japan*
[25]*Department of Physics, Okayama University, Okayama, Okayama 700-8530, Japan*
[26]*Department of Physics, Osaka University, Toyonaka, Osaka 560-0043, Japan*
[27]*Department of Physics, Seoul National University, Seoul 151-742, Korea*
[28]*Department of Systems Engineering, Shizuoka University, Hamamatsu, Shizuoka 432-8561, Japan*
[29]*Department of Informatics in Social Welfare, Shizuoka University of Welfare, Yaizu, Shizuoka 425-8611, Japan*
[30]*Department of Physics, Sungkyunkwan University, Suwon 440-746, Korea*
[31]*Research Center for Neutrino Science, Tohoku University, Sendai, Miyagi 980-8578, Japan*

[*]Present address: Center for Gravitational Wave Physics, Pennsylvania State University, University Park, PA 16802, USA
[†]Present address: Kamioka Observatory, Institute for Cosmic Ray Research, University of Tokyo, Kamioka, Gifu, 506-1205, Japan
[‡]Present address: TRIUMF, Vancouver, British Columbia V6T 2A3, Canada

[32]*Department of Physics, Tokai University, Hiratsuka, Kanagawa 259-1292, Japan*
[33]*Department of Physics, Tokyo Institute for Technology, Meguro, Tokyo 152-8551, Japan*
[34]*University of Tokyo, Tokyo 113-0033, Japan*
[35]*Institute of Experimental Physics, Warsaw University, 00-681 Warsaw, Poland*
[36]*Department of Physics, University of Washington, Seattle, Washington 98195-1560, USA*
(Received 5 April 2006; revised manuscript received 13 June 2006; published 2 August 2006)

We report on the results of a three-flavor oscillation analysis using Super-Kamiokande I atmospheric neutrino data, with the assumption of one mass scale dominance ($\Delta m^2_{12} = 0$). No significant flux change due to matter effect, which occurs when neutrinos propagate inside the Earth for $\theta_{13} \neq 0$, has been seen either in a multi-GeV ν_e-rich sample or in a ν_μ-rich sample. Both normal and inverted mass hierarchy hypotheses are tested and both are consistent with observation. Using Super-Kamiokande data only, 2-dimensional 90% confidence allowed regions are obtained: mixing angles are constrained to $\sin^2\theta_{13} < 0.14$ and $0.37 < \sin^2\theta_{23} < 0.65$ for the normal mass hierarchy. Weaker constraints, $\sin^2\theta_{13} < 0.27$ and $0.37 < \sin^2\theta_{23} < 0.69$, are obtained for the inverted mass hierarchy case.

DOI: 10.1103/PhysRevD.74.032002 PACS numbers: 14.60.Pq, 96.50.S−

I. INTRODUCTION

Recently a number of experiments have shown evidence for oscillations of atmospheric [1–6], solar [7,8], reactor [9], and accelerator neutrinos [10].

In the standard oscillation picture, the three neutrino flavor eigenstates are related to the mass eigenstates by a 3×3 unitary mixing matrix U:

$$|\nu_\alpha\rangle = \sum_{i=1}^{3} U_{\alpha i}|\nu_i\rangle. \tag{1}$$

In this picture, neutrino oscillations can be described by six parameters: two independent $\Delta m^2{}_{ij}$ (Δm^2_{12}, Δm^2_{23}), three mixing angles (θ_{12}, θ_{23}, θ_{13}), and a CP-violating phase δ. The mixing matrix U of Eq. (1) can be written as a product of three rotations, each described by one of the mixing angles:

$$\mathrm{U} = \begin{pmatrix} 1 & 0 & 0 \\ 0 & c_{23} & s_{23} \\ 0 & -s_{23} & c_{23} \end{pmatrix} \begin{pmatrix} c_{13} & 0 & s_{13}e^{-i\delta} \\ 0 & 1 & 0 \\ -s_{13}e^{i\delta} & 0 & c_{13} \end{pmatrix} \times \begin{pmatrix} c_{12} & s_{12} & 0 \\ -s_{12} & c_{12} & 0 \\ 0 & 0 & 1 \end{pmatrix}, \tag{2}$$

where "s" represents sine of the mixing angle and "c" represents cosine.

The "1–2" matrix describes solar mixing; the "2–3" matrix describes atmospheric neutrino mixing. The "1–3" mixing is known to be small; the best current limits on θ_{13} come from the CHOOZ experiment [11].

As yet, the Super-Kamiokande atmospheric neutrino oscillation fits have been done within a two-flavor oscillation framework [5,12]. In this paper, we explore the atmospheric data in the context of a three-flavor analysis.

Among the remaining problems in neutrino physics that can be answered by oscillation experiments are whether θ_{13} is nonzero, and whether the hierarchy is normal or inverted, i.e. whether Δm^2_{23} is positive or negative. At baselines and energies appropriate for atmospheric neutrinos, the signature of a nonzero θ_{13} is a matter-enhanced excess of upward-going electron-like events and possible additional small rate changes of upward-going muon-like events with respect to two-flavor $\nu_\mu \rightarrow \nu_\tau$ transition. The expected effects on electron-like (and muon-like) event rates differ for normal and inverted mass hierarchy cases because the matter effect and the cross section differ for ν_e and $\bar{\nu}_e$.

II. THREE NEUTRINO OSCILLATION WITH ONE MASS SCALE DOMINANT

In general, neutrino oscillations are driven by differences of squared masses, m^2_1, m^2_2, m^2_3. We have adopted the so-called "one mass scale dominance" framework:

$$|m^2_2 - m^2_1| \ll |m^2_3 - m^2_{1,2}|. \tag{3}$$

This approximation is supported by experimental observations of solar, reactor, atmospheric, and accelerator neutrino oscillations. The advantage of this framework is that the number of parameters involved in neutrino oscillations is reduced to three: two mixing angles (θ_{23}, θ_{13}) and one mass squared difference Δm^2,

$$\Delta m^2 \equiv m^2_3 - m^2_{1,2}. \tag{4}$$

The ignored oscillation effects driven by the smaller mass difference $\Delta m^2_{12} \equiv |m^2_2 - m^2_1|$, which might be observed for a neutrino energy of a few hundred MeV, are known to be greatly reduced in the case that the initial flavor flux ratio of ν_μ/ν_e is 2 and $\sin^2 2\theta_{23}$ is close to 1 [13]. For oscillations driven by the dominant Δm^2, a similar "screening" effect holds, but more weakly, because the flavor ratio starts deviating from 2 at 1 GeV and reaches $\sim$3 at 10 GeV. Equation (3) can hold both for $m^2_{1,2} \ll m^2_3$ (normal mass hierarchy) and $m^2_3 \ll m^2_{1,2}$ (inverted mass hierarchy). We present tests of both cases in this paper.

In this framework, in the case of nonzero θ_{13} the neutrino transition and survival probabilities in vacuum, valid

for down-going atmospheric neutrinos, are expressed as

$$\begin{aligned} \mathrm{P}(\nu_e \to \nu_e) &= 1 - \sin^2 2\theta_{13} \sin^2\left(\frac{1.27\Delta m^2 L}{E}\right) \\ \mathrm{P}(\nu_\mu \to \nu_e) &= \mathrm{P}(\nu_e \to \nu_\mu) \\ &= \sin^2\theta_{23} \sin^2 2\theta_{13} \sin^2\left(\frac{1.27\Delta m^2 L}{E}\right) \\ \mathrm{P}(\nu_\mu \to \nu_\mu) &= 1\text{–}4\cos^2\theta_{13}\sin^2\theta_{23}(1 - \cos^2\theta_{13}\sin^2\theta_{23}) \\ &\quad \times \sin^2\left(\frac{1.27\Delta m^2 L}{E}\right) \end{aligned} \tag{5}$$

where L is neutrino travel length in km from the neutrino production point in the atmosphere, E is neutrino energy in GeV, and Δm^2 in eV^2. In the limit of zero θ_{13}, these equations reduce to pure $\nu_\mu \leftrightarrow \nu_\tau$ two-flavor oscillation. Because $\mathrm{P}(\nu_e \to \nu_e)$ in Eq. (5) is a function of $\sin^2 2\theta_{13}$, both $\sin^2\theta_{13} \sim 0$ and $\sin^2\theta_{13} \sim 1$ can satisfy electron flavor disappearance constraints from reactor neutrino experiments. However, $\sin^2\theta_{13} \sim 1$ is inconsistent with an observed large deficit of atmospheric ν_μ because $\mathrm{P}(\nu_\mu \to \nu_\mu)$ in Eq. (5) becomes $\sim$1 for this case. Therefore, $\sin^2\theta_{13} > 0.5$ is not discussed here.

For neutrinos traversing the Earth, oscillation probability is calculated taking into account Earth's matter potential due to the forward scattering amplitude of charged current ν_e and $\bar{\nu}_e$ interactions [14–16]. We adopted a model in which the Earth is well-approximated by four layers of a constant matter density (core 1: $R \leq 1221$ km, $\rho = 13.0$ g/cm^3, core 2: $1221 < R \leq 3480$ km, $\rho = 11.3$ g/cm^3, mantle: $3480 < R \leq 5701$ km, $\rho = 5.0$ g/cm^3, surface: $5701 < R \leq 6371$ km, $\rho = 3.3$ g/cm^3). The method of calculating matter oscillation probabilities in constant density is based on [17].

In constant matter density, $\mathrm{P}(\nu_\mu \to \nu_e)$ can be described by replacing the mixing angle θ_{13} and Δm^2 in Eq. (5) as

$$\begin{aligned} \mathrm{P}(\nu_\mu \to \nu_e) &= \mathrm{P}(\nu_e \to \nu_\mu) \\ &= \sin^2\theta_{23} \sin^2 2\theta_{13}^M \sin^2\left(\frac{1.27\Delta m_M^2 L}{E}\right) \end{aligned} \tag{6}$$

and the effective mixing angle is

$$\begin{aligned} \sin^2 2\theta_{13}^M &= \frac{\sin^2 2\theta_{13}}{(\cos 2\theta_{13} - A_{\mathrm{CC}}/\Delta m^2)^2 + \sin^2 2\theta_{13}} \\ A_{\mathrm{CC}} &= 2\sqrt{2} G_F N_e p, \end{aligned} \tag{7}$$

where G_F is the Fermi constant, N_e is the electron densities in the medium and p is neutrino momentum [18]. The matter potential term A_{CC} has the same absolute value, but opposite sign for neutrinos and antineutrinos. Because of the matter effect, the Mikheyev-Smirnov-Wolfenstein (MSW) resonance happens in that the $\nu_\mu \to \nu_e$ oscillation probability in Eqs. (6) and (7) becomes large at 3–10 GeV neutrino energy even for the case of small θ_{13} [19–22]. To demonstrate the behavior of ν_e oscillations, Fig. 1 shows the transition probability of ν_e to ν_μ after traversing the Earth. Note that for normal mass hierarchy, the ν_e flux is resonantly enhanced, and there is no enhancement for

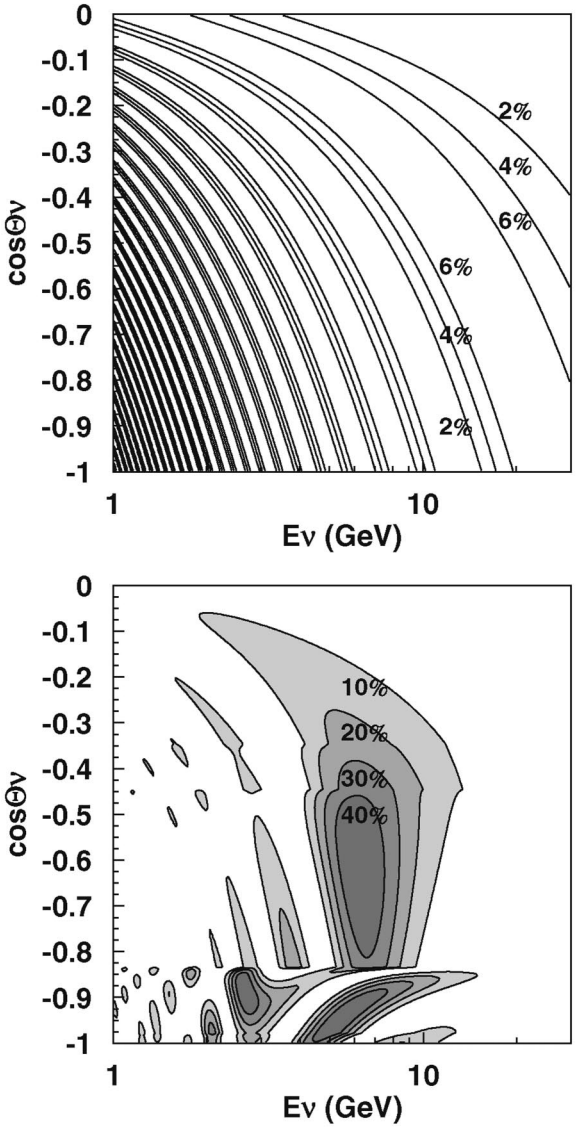

FIG. 1. Oscillation probability of $\nu_e \to \nu_\mu$ (or $\nu_\mu \to \nu_e$) transition. For both figures, the horizontal axis shows neutrino energy and the vertical axis shows the zenith angle of neutrino direction; $\cos\Theta_\nu = -1$ and $\cos\Theta_\nu = 0$ correspond to vertically upward and horizontal directions, respectively. Angles with $\cos\Theta_\nu < -0.84$ correspond to neutrinos passing through the earth core layers. Assumed oscillation parameters are ($\Delta m^2 = 2.5 \times 10^{-3}$ eV^2, $\sin^2\theta_{23} = 0.5$, $\sin^2\theta_{13} = 0.04$). The top figure assumes neutrino oscillation in vacuum and the bottom figure takes into account Earth's matter effect. In the bottom figure, three high probability ($> 40\%$) regions are shown which correspond to the MSW resonance at 3 GeV in the core layer, the MSW resonance at 7 GeV in the mantle layer, and the enhancement due to the core-mantle transition interference [20] at the energy between the two MSW regions.

antineutrinos; the situation is reversed for the inverted mass hierarchy. In matter, the solar and the interference terms modify the ν_e enhancement in the resonance region by less than 5%, justifying our assumption of $\Delta m^2_{12} = 0$.

III. DATA SAMPLE

Super-Kamiokande is a 22.5 kt fiducial mass water Cherenkov detector located at a depth of 2700 m water equivalent in the Kamioka mine, Gifu, Japan. The detector is optically separated into two concentric cylindrical regions. The inner detector (ID) is instrumented with 11 146 20-inch photomultiplier tubes (PMT). The outer detector (OD) is instrumented with 1885 8-inch PMTs. Details of the detector can be found in Ref. [23]. Physical quantities associated with a neutrino event such as the interaction vertex, the number of Cherenkov rings, the direction of each ring, particle identification (PID), momentum, and number of Michel electrons are reconstructed by using hit timing and charge distributions of Cherenkov ring images recorded by PMTs on the ID wall.

Atmospheric neutrino data are categorized into fully-contained (FC), partially-contained (PC), and upward-going muons (UPμ). In the FC events, all of their Cherenkov light is deposited in the ID. In the PC events, there is an exiting particle that deposits visible energy in the OD. Neutrino interactions in the rock below the detector produce UPμ events for which muons either stop in the detector, or pass through the detector. In the present analysis, we use 1489 live-days of FC, PC and 1646 days UPμ neutrino data taken from May 1996 through July 2001 during the Super-Kamiokande I period.

We divide the FC sample into sub-GeV and multi-GeV subsamples according to the visible energy as $E_{\rm vis} < 1.33$ GeV for sub-GeV, $E_{\rm vis} > 1.33$ GeV for multi-GeV where the visible energy of an event is the total energy assuming all Cherenkov light is from electromagnetic showers. The sample is also divided into single-ring and multi-ring by number of reconstructed Cherenkov rings, and into e-like and μ-like by PID of the most energetic ring. Sub- and multi-GeV, e- and μ-like events from the single-ring sample, and sub- and multi-GeV μ-like events from the multi-ring sample are used in the analysis, as for the $\nu_\mu \rightarrow \nu_\tau$ two-flavor oscillation analysis [5]. We also divide the PC sample into ''OD stopping events'' and ''OD through-going events'' according to energy deposited in the OD [12]. Finally, the UPμ sample is divided into upward stopping muons (entering and stopping in the tank) and upward through-going muons (passing through the tank).

As mentioned in the previous section, an excess of upward-going ν_e and/or $\bar{\nu}_e$ in the several GeV region is expected for certain oscillation parameter sets. To improve the sensitivity to this case, a ν_e-enriched sample is selected from the multi-GeV multi-ring e-like sample and is used in addition to the standard oscillation analysis samples. The ν_e-enriched selection is based on a likelihood analysis using PID likelihood, momentum fraction of the most

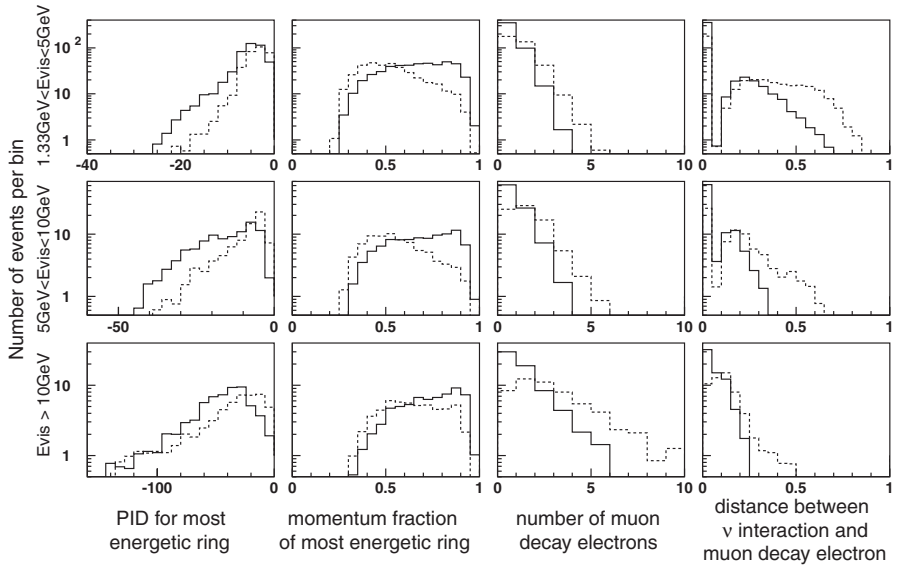

FIG. 2. Livetime normalized MC distributions used in the ν_e-enriched likelihood selection for multi-GeV multi-ring e-like events. Plots correspond to $1.33 < E_{\rm vis} < 5$ GeV, $5 < E_{\rm vis} < 10$ GeV, and $E_{\rm vis} > 10$ GeV from top to bottom. From left to right are shown PID likelihood for the most energetic ring (more negative means more electron-like), momentum fraction of the most energetic ring, number of Michel decay electrons, and square root of distance between decay electron and neutrino interaction vertex divided by visible energy of most energetic ring in $(\mathrm{cm/MeV})^{1/2}$. Solid histograms are $\nu_e + \bar{\nu}_e$ CC, dashed are backgrounds (NC + ν_μCC + $\bar{\nu}_\mu$CC). The ν_e or $\bar{\nu}_e$ CC signals tend to give more electron-like PID and higher momentum fraction. In contrast, backgrounds tend to give more muon decay electrons and the longer decay electron distance due to energetic muons produced by ν_μ or $\bar{\nu}_\mu$CC interactions.

TABLE I. Breakdown of multi-GeV multi-ring e-like events in the MC sample before and after a ν_e-enrichment based on a likelihood analysis. For each interaction mode, the number of events normalized to 1489 live-days and the fraction are shown assuming pure $\nu_\mu \leftrightarrow \nu_\tau$ two-flavor oscillation ($\Delta m^2 = 2.5 \times 10^{-3}$ eV^2, $\sin^2\theta_{23} = 0.5$, $\sin^2\theta_{13} = 0$). Survival efficiency for $\nu_e + \bar{\nu}_e$ CC events is 66.8%.

multi-GeV multi-ring e-like events	$\nu_e + \bar{\nu}_e$ CC	$\nu_\mu + \bar{\nu}_\mu$ CC	NC	total
no likelihood cut	630.8	242.2	258.0	1131.1
	55.8%	21.4%	22.8%	100%
likelihood cut	421.3	49.1	86.8	557.3
	75.6%	8.8%	15.6%	100%
efficiency	66.8%			

energetic ring, number of muon decay electrons, and distance between muon decay electron and primary neutrino interaction position. Figure 2 shows distributions of Monte Carlo (MC) events used to obtain the ν_e-enriched likelihood function. The $\nu_e + \bar{\nu}_e$ charged current (CC) and ν_μ CC + $\bar{\nu}_\mu$CC + neutral current (NC) interactions are separately shown. These distributions are divided into 5 energy regions; 1.33–2.5 GeV, 2.5–5 GeV, 5–10 GeV, 10–20 GeV, and >20 GeV. Each normalized signal (background) distributions forms a probability density function $\mathrm{PDF}^{\mathrm{Sig}}_{i,j}(x_i)$ [$\mathrm{PDF}^{\mathrm{BG}}_{i,j}(x_i)$], where i denotes the four observed variables and j is five energy bins. Then the ν_e-enriched selection criterion for each event is defined as $\sum_{i=1}^{4}\{\log(\mathrm{PDF}^{\mathrm{Sig}}_{i,j}(x_i)) - \log(\mathrm{PDF}^{\mathrm{BG}}_{i,j}(x_i))\} > 0$. As is shown in Table I, the $\nu_e + \bar{\nu}_e$ fraction in the multi-GeV multi-ring e-like sample is improved to 75.6% after the likelihood cut. A summary of the number of observed and expected FC multi-ring e-like events is shown in Table III in the appendix.

IV. OSCILLATION ANALYSIS

The oscillation analysis is performed by comparing data with MC equivalent to 100 years of detector exposure. The atmospheric neutrino flux calculation from [24] and neutrino interaction model (NEUT) [5,25] are used to simulate interactions with the nuclei of water, or in the case of upward muons, the nuclei of the rock surrounding the detector. We use a GEANT-based full detector simulation to generate the MC neutrino events.

We employ a χ^2 test to perform three-flavor oscillation analysis. All events are divided into 37 momentum or energy bins (10 + 5 bins for FC single- and multi-ring e-like, 8 + 4 bins for FC single- and multi-ring μ-like, 4 + 4 bins for OD stopping and OD through-going PC, and 1 + 1 bin for upward stopping and through-going muons). The reconstructed quantities used for momentum binning for the various event classes are: the observed momentum of the charged lepton for FC single-ring e- and μ-like events (P_{lep}), the sum of the energies of the observed rings (reconstructed particles) considering particle mass for FC multi-ring e-like events (E_{tot}), and the sum of visible energies of observed rings for FC multi-ring μ-like and PC events (E_{vis}). Note that the binning of the energy scale differs from that of [5,12], i.e. events in the multi-GeV energy range are divided more finely in order to obtain better sensitivity to Δm^2. Each momentum bin is also divided into 10 bins equally spaced between $\cos\Theta = -1$ and $\cos\Theta = +1$ ($-1 < \cos\Theta < 0$ for UPμ events), where $\cos\Theta$ is the cosine of the zenith angle of the reconstructed particle direction. Table III summarizes the number of observed and expected FC, PC and UPμ events for each bin. The total number of bins is 370. The number of events in each bin is compared with expectation and a χ^2 value is calculated according to a Poisson probability distribution defined by the following expression:

$$\chi^2 = \sum_{n=1}^{370}\Bigg[2\Bigg\{N^n_{\mathrm{exp}}\Bigg(1 + \sum_{i=1}^{45} f^n_i \cdot \epsilon_i\Bigg) - N^n_{\mathrm{obs}}\Bigg\} + 2N^n_{\mathrm{obs}} \ln\Bigg(\frac{N^n_{\mathrm{obs}}}{N^n_{\mathrm{exp}}(1 + \sum_{i=1}^{45} f^n_i \cdot \epsilon_i)}\Bigg)\Bigg] + \sum_{i=1}^{43}\Bigg(\frac{\epsilon_i}{\sigma_i}\Bigg)^2, \tag{8}$$

where

N^n_{obs} = Number of observed events in nth bin

N^n_{exp} = Number of expected events in nth bin

ϵ_i = ith systematic error term

f^n_i = systematic error coefficient

σ_i = 1 sigma value of systematic error

TABLE II. Sources of systematic errors in addition to those in common with the $\nu_\mu \leftrightarrow \nu_\tau$ oscillation analysis [5]. Non-ν backgrounds in UPμ samples are treated as fitting parameters in this analysis, while they are taken into account by modifying statistical error size in Ref. [5].

	Estimated error size (%)
Non-ν background [a]	
upward through-going muons	3.0
upward stopping muons	17
Non-(ν_e CC) background [b]	
multi-GeV single-ring e-like	14
multi-GeV multi-ring e-like	20
sample normalization of multi-GeV multi-ring e-like	free
OD stopping PC/through-going PC separation	12

[a]Cosmic ray muon backgrounds are assigned as systematic errors to the most horizontal zenith angle bins ($-0.1 < \cos\Theta < 0$).
[b]Contamination of ν_μ CC interactions.

The expectation $N^n_{\rm exp}$ is calculated using MC events corrected by oscillation probability. Here, systematic uncertainty factors explicitly multiply the $N^n_{\rm exp}$. We considered 45 systematic error sources, which come from detector calibration, neutrino flux, neutrino interactions and event selection. Most of them are in common with those listed in [5], and additional systematic uncertainties related to backgrounds of the e-like sample and upward-going muons, and sample normalization of e-like events are estimated as listed in Table II. Among 45 errors, only 43 contribute to the χ^2, because the overall normalization and sample normalization of multi-GeV multi-ring e-like are allowed to be free. The f^n_i values are calculated and tabulated in advance for every bin and for every systematic error source. A global scan is carried out on a $[\log_{10}(\Delta m^2), \sin^2\theta_{23}, \sin^2\theta_{13}]$ grid minimizing χ^2 with respect to 45 systematic error parameters. The ϵ_i values are fit in order to minimize the χ^2 value. We used ϵ_i such that the first derivative of χ^2 with respect to ϵ_i is zero ($\frac{\delta\chi^2}{\delta\epsilon_i} = 0$), which can be obtained by solving linear equations [26]. Since this equation has nonlinear terms for our χ^2 definition, we use an approximate solution obtained by an iteration method.

A global scan of the oscillation parameter grid assuming normal mass hierarchy results in a minimum χ^2 value of $\chi^2_{\rm min} = 377.39/368$ DOF at the grid point $(\Delta m^2, \sin^2\theta_{23}, \sin^2\theta_{13}) = (2.5 \times 10^{-3}\ {\rm eV}^2, 0.5, 0.0)$, which is consistent with $\nu_\mu \leftrightarrow \nu_\tau$ two-flavor oscillation. Figure 3 shows the zenith angle distribution of each data sample overlaid with nonoscillated and best-fit expectations. The fitted distributions agree well with data. Figure 4 shows the up-down asymmetry as a function of particle momentum or total energy. The asymmetry (UP − DOWN)/(UP + DOWN) distributions are consistent with the fitted expectation. No significant excess due to matter effect is seen in the upward-going multi-GeV e-like sample, suggesting no evidence for nonzero θ_{13}. Allowed regions of neutrino oscillation parameters are obtained based on the χ^2 defined in Eq. (8). The 2-dimensional 90% (99%) confidence level allowed region is defined to be $\chi^2 = \chi^2_{\rm min} + 4.6(9.2)$ and obtained as shown in Fig. 5. The region corresponding to $\sin^2\theta_{13} < 0.14$ and $0.37 < \sin^2\theta_{23} < 0.65$ is allowed at 90% confidence level.

Finally, we tested the inverted mass hierarchy hypothesis. Water Cherenkov detectors, such as Super-K, cannot discriminate between neutrinos and antineutrinos on an event-by-event basis. However, mass hierarchy affects the expected number of e-like events. Because of the lower cross section of $\bar{\nu}_e$, an enhancement of the multi-GeV ν_e-rich sample is expected to be suppressed and therefore the constraint on θ_{13} will be weakened for the inverted mass hierarchy case. Allowed regions assuming inverted mass hierarchy are also obtained and shown in Fig. 6. $\chi^2_{\rm min} = 377.31/368$ DOF is obtained at the grid point of $(\Delta m^2, \sin^2\theta_{23}, \sin^2\theta_{13}) = (-2.5 \times 10^{-3}\ {\rm eV}^2, 0.525, 0.006\,25)$. There is little difference in the $\chi^2_{\rm min}$ values of the normal and inverted hierarchy cases; therefore both hypotheses are allowed by Super-K data. Figure 7 shows

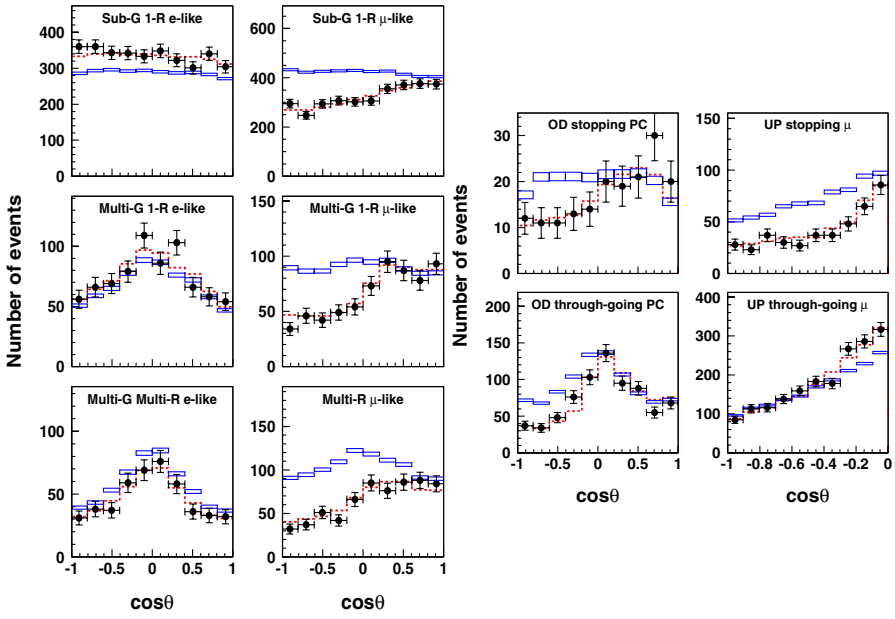

FIG. 3 (color online). Zenith angle distributions of FC e-like, μ-like, PC, and UPμ are shown for data (filled circles with statistical error bars), MC distributions without oscillation (boxes) and best-fit distributions (dashed). The nonoscillated MC shows the distribution without fitting and the box height shows the statistical error. In the case of nonzero θ_{13}, matter-enhanced excess of electron-like events is expected in the zenith angle of $-1 < \cos\theta < -0.2$ regions in the multi-GeV 1-ring and multi-ring electron-like samples. The ν_μ in the resonance regions populate mainly in the multi-GeV single-ring muon, multi-ring muon, two PC, and UP stopping μ samples.

$\chi^2 - \chi^2_{\rm min}$ distributions projected to $\sin^2\theta_{13}$, in which minimum χ^2 values for each Δm^2 and $\sin^2\theta_{23}$ are plotted. It is shown that the $\chi^2 - \chi^2_{\rm min}$ distribution for the inverted hierarchy is flatter and a larger $\sin^2\theta_{13}$ value is allowed. The constraint on $\sin^2\theta_{13}$ is weaker for the inverted hierarchy case; $\sin^2\theta_{13} < 0.27$ and $0.37 < \sin^2\theta_{23} < 0.69$ are allowed at 90% confidence level.

The present analysis obtained upper limits on θ_{13} which confirms CHOOZ experiment [11] (shown by Figs. 5 and

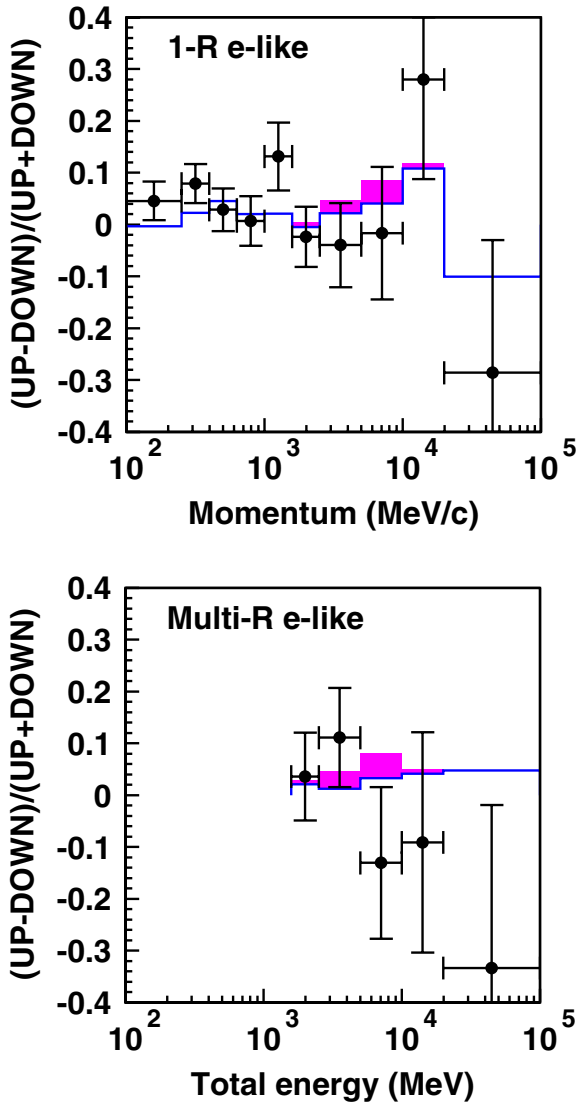

FIG. 4 (color online). Asymmetry (UP − DOWN)/(UP + DOWN) as a function of particle momentum for FC single-ring e-like events (top) and as a function of total energy for FC multi-ring e-like events (bottom), where UP (DOWN) refers to the number of events in $-1.0 < \cos\Theta < -0.2$ ($0.2 < \cos\Theta < 1.0$). Filled circles represent data (error bars are statistical), the line represents best-fit distributions under a normal hierarchy assumption, and the filled area on the best-fit line represents the expected excess due to matter effect for $(\Delta m^2, \sin^2\theta_{23}, \sin^2\theta_{13}) = (2.5 \times 10^{-3}\ \mathrm{eV}^2, 0.5, 0.04)$.

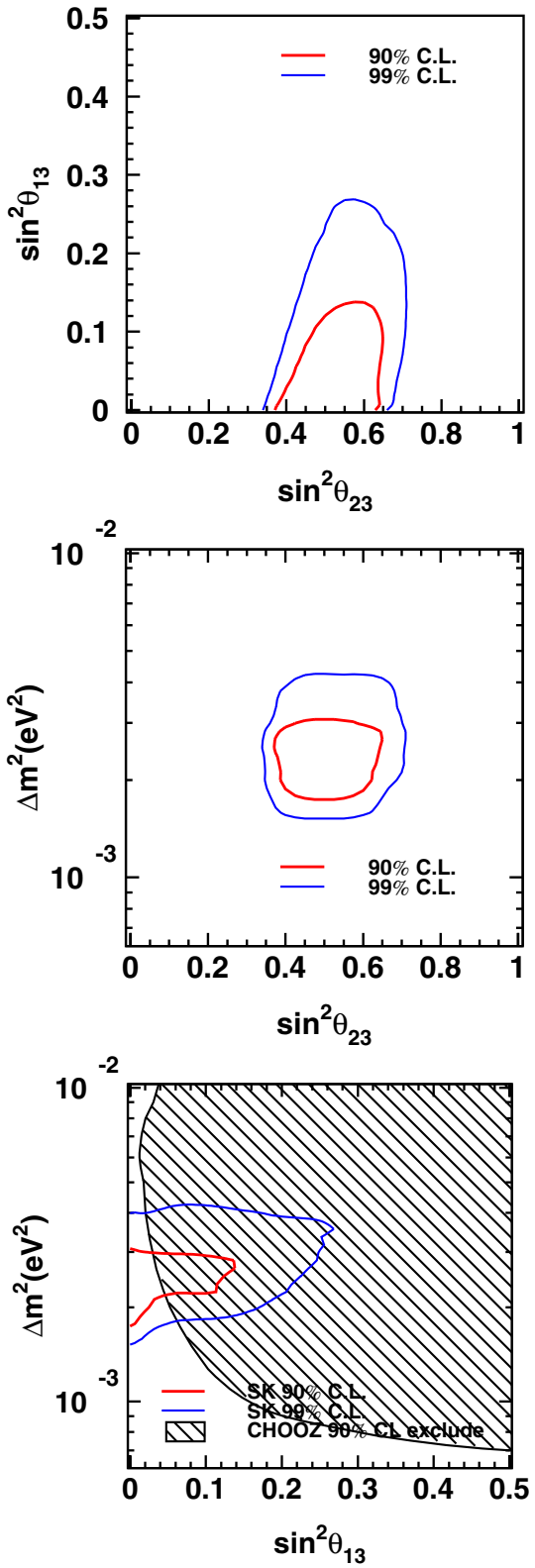

FIG. 5 (color online). 90% (thick line) and 99% (thin line) confidence level allowed regions are shown in $\sin^2\theta_{13}$ vs $\sin^2\theta_{23}$ (top), Δm^2 vs $\sin^2\theta_{23}$ (middle), and Δm^2 vs $\sin^2\theta_{13}$ (bottom). Normal mass hierarchy ($\Delta m^2 > 0$) is assumed. The shaded area in the bottom figure shows the region excluded by the CHOOZ reactor neutrino experiment.

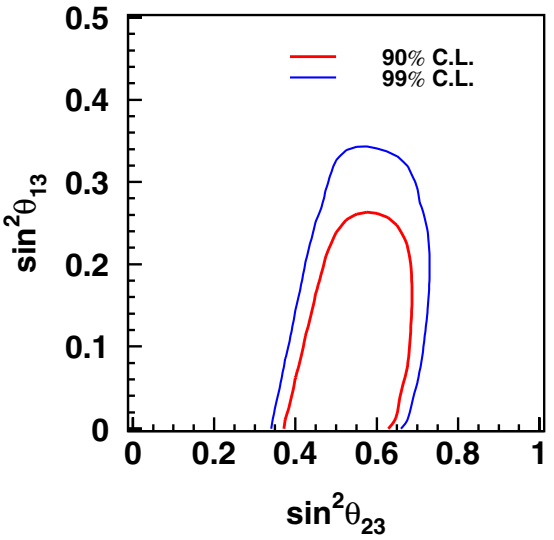

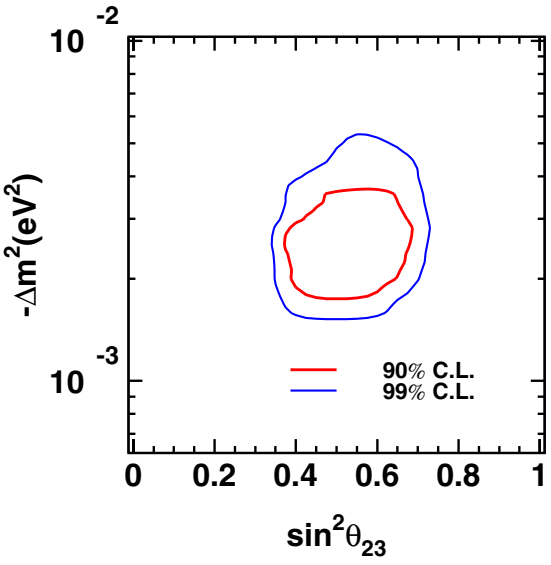

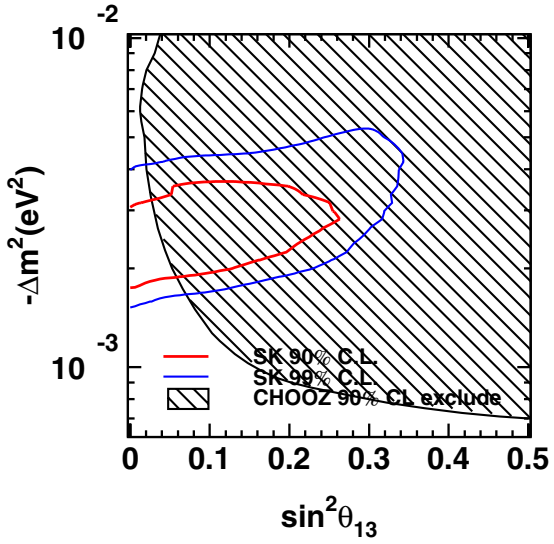

FIG. 6 (color online). 90% (thick line) and 99% (thin line) confidence level allowed regions assuming inverted mass hierarchy ($\Delta m^2 < 0$), shown in the same orientation as in Fig. 5.

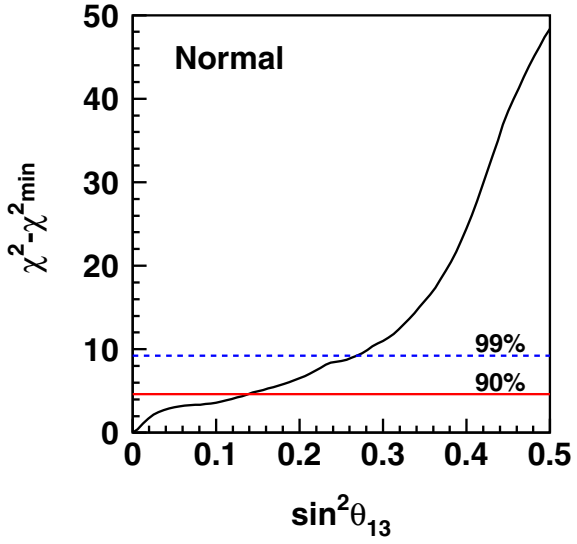

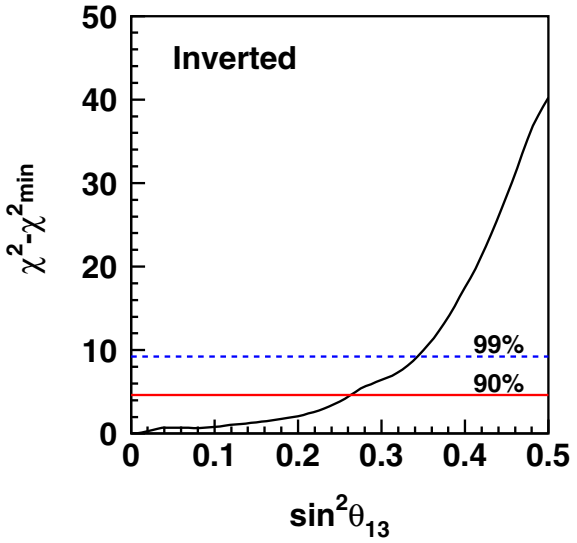

FIG. 7 (color online). For normal (top) and inverted (bottom) mass hierarchy assumption, $\chi^2 - \chi^2_{\text{min}}$ are shown as a function of $\sin^2\theta_{13}$. Minimum χ^2 values for each Δm^2 and $\sin^2\theta_{23}$ are selected and plotted at each $\sin^2\theta_{13}$. Solid (dashed) lines show 2-dimensional 90% (99%) confidence level allowed regions.

6) and Palo Verde [27]. These limits are also consistent with the recent result by the K2K experiment [28] giving the upper limit of $\sin^2\theta_{13} \sim 0.06$ at $\Delta m^2 = 2.8 \times 10^{-3}$ eV^2, assuming $\sin^2\theta_{23} = 0.5$.

V. CONCLUSION

In summary, a three-flavor oscillation analysis assuming one mass scale dominance ($\Delta m^2_{12} = 0$) was performed with Super-Kamiokande I FC + PC + UPμ combined data set. A multi-ring e-like sample, selected using a likelihood method, was newly introduced to increase the statistics of electron neutrinos and improve the sensitivity to θ_{13}. The best-fitted parameters for three-flavor oscillation

becomes $(\Delta m^2, \sin^2\theta_{23}, \sin^2\theta_{13}) = (2.5 \times 10^{-3}\ \mathrm{eV}^2, 0.5, 0.0)$ and the region of $\sin^2\theta_{13} < 0.14$ and $0.37 < \sin^2\theta_{23} < 0.65$ is allowed at 90% confidence level, assuming normal mass hierarchy. We also tested the inverted mass hierarchy case: a wider region, $\sin^2\theta_{13} < 0.27$ and $0.37 < \sin^2\theta_{23} < 0.69$ is allowed at 90% confidence level. Both mass hierarchy hypotheses agree with our data. We obtained the upper limit on θ_{13}, which is consistent with CHOOZ, Palo Verde, and K2K experiments, by using high statistics atmospheric neutrinos. In contrast to these past experiments, the earth matter effect plays an important role in the analysis.

ACKNOWLEDGMENTS

We gratefully acknowledge the cooperation of the Kamioka Mining and Smelting Company. The Super-Kamiokande experiment has been built and operated from funding by the Japanese Ministry of Education, Culture, Sports, Science and Technology, the United States Department of Energy, and the U.S. National Science Foundation. Some of us have been supported by funds from the Korean Research Foundation (BK21) and the Korea Science and Engineering Foundation, the Polish Committee for Scientific Research (grant No. 1P03B08227), Japan Society for the Promotion of Science, and Research Corporation.

APPENDIX

Table III summarizes the number of observed and expected FC, PC and UPμ events for each bin. The Monte Carlo prediction does not include neutrino oscillations. These binned data are used in the oscillation analysis.

TABLE III. Summary of the number of observed (MC expected) FC, PC and UPμ events for each bin. Neutrino oscillation is not included in the MC prediction. Roman numbers I, II, ... X represent zenith angle regions $-1 < \cos\Theta < -0.8$, $-0.8 < \cos\Theta < -0.6$, ... and $0.8 < \cos\Theta < 1.0$ respectively for FC and PC events, $-1 < \cos\Theta < -0.9$, $-0.9 < \cos\Theta < -0.8$, ... and $0.1 < \cos\Theta < 0.0$ respectively for upward stopping and through-going muon events. The numbers 1 to 5 in the P_{lep} column correspond to the momentum ranges <250, 250–400, 400–630, 630–1000 and >1000 MeV/c for sub-GeV samples and the numbers 6 to 10 correspond to <2.5, 2.5–5.0, 5.0–10, 10–20 and >20 GeV/c for multi-GeV samples. The letters a to f in the E_{tot} and E_{vis} columns correspond to energy ranges 0.2–1.33, 1.33–2.5, 2.5–5.0, 5.0–10, 10–20, >20 GeV.

					FC single-ring e-like					
P_{lep}	I	II	III	IV	V	VI	VII	IIX	IX	X
1	114(79.3)	95(83.3)	74(81.4)	94(82.0)	88(84.0)	91(79.8)	79(79.5)	74(84.2)	91(81.5)	100(82.9)
2	96(75.6)	93(71.7)	96(73.2)	90(69.4)	89(68.4)	85(68.8)	85(69.5)	74(67.2)	83(71.1)	78(69.7)
3	76(64.2)	80(66.9)	80(65.8)	69(63.6)	72(64.6)	60(64.1)	69(62.4)	71(61.7)	85(59.7)	63(57.5)
4	48(45.4)	57(47.9)	62(50.1)	52(50.9)	60(51.6)	74(51.6)	55(50.8)	58(49.1)	60(46.5)	43(42.5)
5	26(21.7)	35(23.2)	31(25.1)	37(25.8)	24(25.6)	38(25.9)	34(25.0)	24(26.1)	21(23.6)	20(18.5)
6	33(29.3)	35(33.2)	41(34.9)	37(39.7)	46(42.8)	49(43.9)	49(40.7)	32(39.5)	36(32.0)	36(27.3)
7	10(13.8)	20(16.6)	15(18.4)	28(23.5)	36(26.6)	19(24.2)	28(22.0)	24(19.9)	18(17.2)	9(12.4)
8	9(5.27)	5(5.40)	10(7.49)	6(9.42)	14(12.4)	11(11.8)	16(8.38)	8(8.26)	2(5.87)	5(4.18)
9	2(1.47)	4(2.83)	3(2.62)	7(3.73)	7(4.38)	6(4.83)	6(3.38)	1(2.63)	1(1.71)	1(1.63)
10	2(0.86)	2(0.86)	0(1.63)	1(1.26)	6(2.40)	1(2.16)	4(1.68)	1(1.79)	1(1.23)	3(1.26)
					FC single-ring μ-like					
P_{lep}	I	II	III	IV	V	VI	VII	IIX	IX	X
1	36(54.7)	40(53.7)	39(54.4)	37(55.1)	35(55.8)	34(53.8)	35(53.5)	45(53.6)	48(52.6)	46(52.1)
2	86(124)	77(123)	99(123)	86(122)	87(119)	80(120)	91(123)	85(118)	94(116)	76(121)
3	94(119)	60(112)	81(113)	94(116)	87(113)	84(113)	116(113)	119(112)	97(108)	118(105)
4	52(91.1)	48(88.0)	53(90.5)	53(91.0)	68(94.7)	68(91.1)	72(89.6)	81(88.2)	91(84.5)	86(82.9)
5	27(43.4)	22(45.9)	22(44.9)	37(44.5)	25(47.0)	40(47.5)	41(47.9)	41(42.6)	46(44.0)	48(43.6)
6	27(58.8)	35(57.3)	29(59.6)	32(61.6)	35(62.3)	57(63.2)	66(64.4)	69(59.6)	49(55.1)	56(54.0)
7	4(26.1)	10(24.9)	12(23.8)	15(27.3)	16(30.7)	15(28.3)	27(28.6)	16(24.6)	25(25.3)	33(26.8)
8–10	3(4.61)	1(4.21)	1(3.11)	2(3.66)	3(3.36)	1(3.14)	2(3.17)	2(4.19)	4(4.16)	4(4.04)
					FC multi-ring e-like					
E_{tot}	I	II	III	IV	V	VI	VII	IIX	IX	X
b	16(16.9)	18(18.1)	16(21.2)	22(26.9)	26(27.8)	31(27.6)	23(24.0)	19(22.1)	14(16.8)	11(16.0)
c	9(13.4)	12(14.9)	13(18.9)	26(22.4)	21(28.2)	22(28.1)	15(22.2)	11(17.9)	10(14.2)	12(12.8)
d	4(5.77)	3(6.40)	6(8.44)	7(11.3)	12(15.1)	14(16.0)	13(12.4)	3(7.28)	4(6.20)	6(4.77)
e	2(2.17)	4(2.71)	1(2.83)	3(5.05)	5(7.61)	4(8.38)	6(5.19)	2(3.74)	3(1.87)	1(2.07)

TABLE III. (*Continued*)

					FC single-ring e-like					
P_{lep}	I	II	III	IV	V	VI	VII	IIX	IX	X
f	0(0.89)	1(1.11)	1(1.68)	1(1.75)	5(4.00)	5(4.70)	1(2.33)	1(0.98)	2(0.89)	2(1.21)
					FC multi-ring μ-like					
E_{vis}	I	II	III	IV	V	VI	VII	IIX	IX	X
a	14(27.6)	8(31.2)	20(33.4)	14(33.7)	25(36.1)	16(35.6)	21(34.1)	32(32.9)	29(28.9)	29(29.1)
b	11(33.2)	14(33.6)	16(36.7)	19(39.9)	20(43.9)	33(43.0)	28(40.7)	31(40.7)	30(33.8)	25(32.5)
c	6(22.4)	11(22.8)	11(23.5)	7(27.5)	13(31.6)	20(28.8)	19(28.0)	17(24.8)	23(22.4)	19(20.4)
d–f	1(7.68)	4(6.88)	4(6.73)	2(8.28)	8(10.8)	16(10.9)	8(8.49)	6(7.81)	6(6.29)	11(7.92)
					OD stopping PC					
E_{vis}	I	II	III	IV	V	VI	VII	IIX	IX	X
a	5(4.26)	2(3.53)	2(3.67)	2(4.29)	1(4.98)	5(4.14)	5(4.26)	6(4.14)	9(3.72)	5(3.78)
b	2(4.38)	2(7.23)	3(6.67)	4(5.18)	6(5.81)	2(6.01)	3(6.85)	5(6.76)	9(6.42)	5(4.29)
c	4(4.18)	7(5.61)	3(6.95)	1(6.88)	2(6.02)	5(6.28)	7(5.89)	4(6.57)	4(6.55)	8(4.63)
d–f	1(4.30)	0(4.63)	3(3.81)	6(4.75)	5(4.08)	8(5.16)	4(4.62)	6(4.33)	8(3.56)	2(2.90)
					OD through-going PC					
E_{vis}	I	II	III	IV	V	VI	VII	IIX	IX	X
a	5(9.90)	9(5.69)	10(8.48)	9(11.2)	9 (13.5)	9(15.1)	11(13.3)	10(8.53)	10(7.13)	7(9.55)
b	4(13.9)	6(14.0)	10(17.3)	21(22.1)	18(25.2)	18(25.9)	12(19.9)	22(17.9)	11(14.0)	20(14.7)
c	8(18.7)	6(20.9)	12(26.1)	15(32.4)	20(36.9)	48(40.2)	36(34.5)	27(24.1)	11(21.8)	18(22.2)
d–f	20(29.4)	13(27.2)	16(31.5)	31(38.4)	56(58.2)	61(55.6)	36(39.1)	29(30.7)	23(26.5)	23(26.2)
					Upward stopping muon					
	28(51.2)	23(54.1)	37(56.7)	30(65.0)	27(67.6)	37(68.2)	37(78.9)	48(81.0)	65(94.0)	85.7(96.9)
					Upward through-going muon					
	85(96.1)	113(115)	116(122)	138(137)	159(146)	183(169)	178(187)	267(211)	286(229)	316.6(257)

[1] R. Becker-Szendy *et al.*, Phys. Rev. D **46**, 3720 (1992).
[2] Y. Fukuda *et al.* (Kamiokande), Phys. Lett. B **335**, 237 (1994).
[3] M. Ambrosio *et al.* (MACRO), Phys. Lett. B **566**, 35 (2003).
[4] W. W. M. Allison *et al.* (Soudan-2), Phys. Rev. D **72**, 052005 (2005).
[5] Y. Ashie *et al.* (Super-Kamiokande), Phys. Rev. D **71**, 112005 (2005).
[6] P. Adamson *et al.* (MINOS), Phys. Rev. D **73**, 072002 (2006).
[7] M. B. Smy *et al.* (Super-Kamiokande), Phys. Rev. D **69**, 011104 (2004).
[8] S. N. Ahmed *et al.* (SNO), Phys. Rev. Lett. **92**, 181301 (2004).
[9] M. Apollonio *et al.* Eur. Phys. J. C **27**, 331 (2003).
[10] E. Aliu *et al.* (K2K), Phys. Rev. Lett. **94**, 081802 (2005).
[11] M. Apollonio *et al.* (CHOOZ), Phys. Lett. B **466**, 415 (1999).
[12] Y. Ashie *et al.* (Super-Kamiokande), Phys. Rev. Lett. **93**, 101801 (2004).
[13] O. L. G. Peres and A. Y. Smirnov, Nucl. Phys. **B680**, 479 (2004).
[14] S. P. Mikheyev and A. Y. Smirnov, Yad. Fiz. **42**, 1441 (1985).
[15] S. P. Mikheyev and A. Y. Smirnov, Nuovo Cimento Soc. Ital. Fis. C **9**, 17 (1986).
[16] L. Wolfenstein, Phys. Rev. D **20**, 2634 (1979).
[17] V. D. Barger, K. Whisnant, S. Pakvasa, and R. J. N. Phillips, Phys. Rev. D **22**, 2718 (1980).
[18] C. Giunti, C. W. Kim, and M. Monteno, Nucl. Phys. **B521**, 3 (1998).
[19] E. K. Akhmedov, A. Dighe, P. Lipari, and A. Y. Smirnov, Nucl. Phys. **B542**, 3 (1999).
[20] M. Chizhov, M. Maris, and S. T. Petcov, hep-ph/9810501.
[21] M. C. Gonzalez-Garcia and M. Maltoni, Eur. Phys. J. C **26**, 417 (2003).
[22] J. Bernabeu, S. Palomares Ruiz, and S. T. Petcov, Nucl. Phys. **B669**, 255 (2003).
[23] Y. Fukuda *et al.*, Nucl. Instrum. Methods Phys. Res., Sect. A **501**, 418 (2003).
[24] M. Honda, T. Kajita, K. Kasahara, and S. Midorikawa, Phys. Rev. D **70**, 043008 (2004).
[25] Y. Hayato, Nucl. Phys. B, Proc. Suppl. **112**, 171 (2002).
[26] G. L. Fogli, E. Lisi, A. Marrone, D. Montanino, and A. Palazzo, Phys. Rev. D **66**, 053010 (2002).
[27] A. Piepke (Palo Verde), Prog. Part. Nucl. Phys. **48**, 113 (2002).
[28] S. Yamamoto *et al.* (K2K), Phys. Rev. Lett. **96**, 181801 (2006).